



Global transcriptome study of Dip2B-deficient mouse embryonic lung fibroblast reveals its important roles in cell proliferation and development



Salah Adlat^a, Rajiv Kumar Sah^a, Farooq Hayel^a, Yang Chen^a, Fatoumata Binta Bah^a, Mahmoud Al-Azab^c, Noor Bahadar^a, May Myint^a, Zin Mar Oo^a, MI Nasser^b, Luqing Zhang^d, Xuechao Feng^{a,b,*}, Yaowu Zheng^{a,b,*}

^a Transgenic Research Center, School of Life Sciences, Northeast Normal University, Changchun, Jilin 130024, China

^b Key Laboratory of Molecular Epigenetics of Ministry of Education, School of Life Sciences, Northeast Normal University, Changchun, Jilin 130024, China

^c Department of Immunology, Guangzhou Institute of Pediatrics, Guangzhou Women and Children's Medical Centre, Guangzhou Medical University, Guangzhou 510623, China

^d Cardiovascular Research Institute, University of California, San Francisco, CA 94158, USA

ARTICLE INFO

Article history:

Received 24 March 2020

Received in revised form 20 August 2020

Accepted 29 August 2020

Available online 5 September 2020

Keywords:

Dip2B knockout

MELFs

Transcriptome

DEG

Gene ontology

KEGG

ABSTRACT

Disco-interacting protein 2 homolog B (Dip2B) is a member of Dip2 family encoded by *Dip2b* gene. Dip2B has been reported to regulate murine epithelial KIT⁺ progenitor cell expansion and differentiation epigenetically via exosomal miRNA targeting during salivary gland organogenesis. However, its molecular functions, cellular activities and biological process remain unstudied. Here, we investigated the transcriptome of Dip2B-deficient mouse embryonic lung fibroblasts (MELFs) isolated from E14.5 embryos by RNA-Seq. Expression profiling identified 1369 and 1104 differentially expressed genes (DEGs) from *Dip2b*^{-/-} and *Dip2b*^{+/-} MELFs in comparisons to wild-type (*Dip2b*^{+/+}). Functional clustering of DEGs revealed that many gene ontology terms belong to membrane activities such as 'integral component of plasma membrane', and 'ion channel activity', suggesting possible roles of Dip2B in membrane integrity and membrane function. KEGG pathway analysis revealed that multiple metabolic pathways are affected in *Dip2b*^{-/-} and *Dip2b*^{+/-} when compared to *Dip2b*^{+/+} MELFs. These include 'protein digestion and absorption', 'pancreatic secretion' and 'steroid hormone synthesis pathway'. These results suggest that Dip2B may play important roles in metabolism. Molecular function analysis shows transcription factors including *Hox*-genes, bHLH-genes, and Forkhead-genes are significantly down-regulated in *Dip2b*^{-/-} MELFs. These genes are critical in embryo development and cell differentiation. In addition, Dip2B-deficient MELFs demonstrated a reduction in cell proliferation and migration, and an increase in apoptosis. All results indicate that Dip2B plays multiple roles in cell proliferation, migration and apoptosis during embryogenesis and may participate in control of metabolism. This study provides valuable information for further understanding of the function and regulatory mechanisms of Dip2B.

© 2020 The Authors. Published by Elsevier B.V. on behalf of Research Network of Computational and Structural Biotechnology. This is an open access article under the CC BY-NC-ND license (<http://creativecommons.org/licenses/by-nc-nd/4.0/>).

1. Introduction

Disco gene was identified as a transcription factor with two C2H2 type zinc finger domains that involve neuronal connection in visual system of *Drosophila melanogaster* [1–2]. By using yeast two-hybrid system, Mukhopadhyay et al. [3] identified a protein that interacts with Disco and named disco-interacting protein 2 (Dip2). Dip2 is highly conserved from insects to mammals and

evolved into three different proteins, DIP2A, DIP2B and DIP2C in mammals [3]. Based on amino acid sequences, Dip2B has three putative functional domains, a binding domain for the transcriptional regulator DMAP1 (DNMT1-associated protein 1), an AMP-binding domain and an adenylate-forming domain [4]. Study suggests that Dip2B may play important roles in DNA methylation and metabolism. Dip2B may epigenetically control cell proliferation and differentiation through DNA methylation [4]. Dip2B deficiency has been associated with mental retardation and developmental delay [4,5]. A small RNA miR-133b-3p can down-regulate Dip2B and epigenetically repress genes for KIT⁺K5 progenitor cell expansion [6]. A correlation in methylation status between colorectal cancer and aberrant miR-133b expression was also reported [7].

* Corresponding authors at: Transgenic Research Center, School of Life Sciences, Northeast Normal University, Changchun, Jilin 130024, China.

E-mail addresses: fengxc997@nenu.edu.cn (X. Feng), zhengyw442@nenu.edu.cn (Y. Zheng).

However, the mechanism underlining most of Dip2B's roles including on cell proliferation, cell differentiation are still not clear.

RNA sequencing (RNA-Seq) takes advantage of the second-generation sequencing technology and is a powerful approach for studying global gene expression profile in a particular cell or tissue. It helps us to understand the regulatory network of genes and pathways [8,9]. Fibroblasts cells were identified as ubiquitous mesenchymal cells that play many essential roles including tissue repair and wound healing [10]. Embryonic fibroblasts are highly diversified and have potential to differentiate into different cell types. Mouse embryonic lung fibroblasts (MELFs) cells from genetically manipulated mouse models have been used to study the molecular mechanism of genes and their regulatory networks, especially those genes that their ablations resulted in mouse prenatal lethality. To explore the potential role of Dip2B, MELFs were isolated from embryos of homozygous knockout (*Dip2b*^{-/-}), heterozygous (*Dip2b*^{+/-}) and wild type (*Dip2b*^{+/+}) at E14.5. Genes and pathways under Dip2B regulation were investigated.

2. Materials and methods

2.1. Animals

Mouse study has been approved by Institutional Animal Care and Use Committee for Animal Experimental Ethics Committee of Northeast Normal University with approval number of (NENU/IACUC, AP2018011) and carried out in accordance with the *Guide for Care and Use of Laboratory Animals of National Institutes of Health* as well. Mice were housed in a pathogen-free facility in Northeast Normal University with temperature at 21 ± 1 °C, humidity 30–60%, 12:12 light/dark cycles and free access to water and food.

2.2. Isolation and culture of lung MELFs

MELFs were isolated from mouse embryos obtained by intercrossing of *Dip2b*^{+/-} transgenic mice. *Dip2b*^{+/-} pregnant mouse at E14.5 day post-coitus (p.c.) was euthanized by cervical dislocation and soaked in 70% ethanol for 5 min, then the uterine horns were dissected out and rinsed in 70% EtOH. Uterine horns were then transferred into petri dish and the embryos were separated individually. Visceral organs of each embryo were removed except lungs. Lungs were washed in 1 × PBS and placed in a new Petri dish. Lung tissues were gently minced using a sterile razor blade till possible to pipette. The tissues were then incubated with 0.25% trypsin (Sigma Aldrich) at 37 °C. Trypsin was inactivated 15 min later by adding Dulbecco's modified Eagle's medium (DMEM) (Gibco, Shanghai, China) containing 10% fetal bovine serum (Sigma, St Louis, USA) and 1% penicillin/streptomycin (Invitrogen Life Technologies, USA). Plates were coated with 0.2% gelatin (Gelatin from bovine skin, Type B, Sigma) for 2 h. The cells were then cultured at 37 °C in a humidified incubator with 5% CO₂.

2.3. Hematoxylin and eosin staining (H&E)

Mice embryos from E19.5 were dissected out from uterus and fixed with 4% paraformaldehyde (PFA) (Sigma-Aldrich; EMD Millipore) for overnight at 4 °C. Fixed tissues were then washed three times in 1x PBS and processed in 70% ethanol. Tissues were dehydrated with a series of graded alcohols, cleared in xylene, and embedded in paraffin. Six-μm thick sections were obtained, mounted on glass slides and stained with Hematoxylin and eosin using standard protocol. Images were taken using microscope (Olympus, Tokyo, Japan).

2.4. Cell proliferation assay by MTT

Methylthiazolyldiphenyl-tetrazolium (MTT, Sigma) test was performed on *Dip2b*^{-/-}, *Dip2b*^{+/-} and *Dip2b*^{+/+} MELFs to measure the proliferation and cell viability. MELFs were detached in 0.25% trypsin/EDTA and seeded into 96-well plates with 5 × 10³ cells per well in 200 μl DMEM containing 10% FBS. Cells were incubated at 37 °C and 5% CO₂ for 24 h and allowed to grow to 70–80% confluence. Then 20 μl of MTT (5 mg/ml in 1 × PBS) was added to each well and incubated for 4hrs. The medium was discarded and 100 μl of dimethyl sulfoxide (DMSO) added to each well. Optical density was analyzed at 490 nm using (BioTek Instruments, Winooski, VT). A total of 4 replicate for each sample was prepared and experiment repeated 3 times.

2.5. Cell apoptosis analysis by FITC-Annexin-V and PI

Apoptosis was detected using FITC-Annexin-V and PI staining kit (Cat #630109, Takara, Japan) according to manufacturer's instructions. Briefly, *Dip2b*^{-/-}, *Dip2b*^{+/-} and WT MELFs were seeded in 6-well plates at a concentration of 3 × 10⁵ cells/well. MELFs were trypsinized and washed twice with 1X PBS. A 5 μl Annexin V-FITC and 10 μl propidium iodide (PI) at 50 μg/ml in 1 × binding buffer (10 mM HEPES/pH 7.4, 140 mM NaOH, 2.5 mM CaCl₂) were added for 15 min at room temperature in the dark. Apoptotic cells were analyzed using a Becton-Dickinson FACSscan cytofluorometer (Mansfield, MA). Both early (Annexin V-positive, PI negative) and late (Annexin V-positive and PI-positive) were considered as apoptotic cells.

2.6. Cell cycle analysis

Dip2b^{+/+}, *Dip2b*^{+/-} and *Dip2b*^{-/-} MELFs were seeded in 6-well plates at a density of 2 × 10⁵ cells/well. Cells were trypsinized and washed twice with 1 × PBS. Then cells were fixed with 70% ice-cold EtOH overnight. Fixed cells were treated with RNase (200 μg/ml) for 2hrs at RT, followed by staining with 500 μl PI (50 μg/ml) (Cat#630109, Takara, Japan). Cells were transferred to FACS tubes and incubated for 30 min at RT in dark. Afterwards, cells were subjected to FACS analysis using Caliber flow cytometer (Becton Dickinson, USA). Dead cells and cell debris were excluded.

2.7. Cell migration assay

Cells were grown in 6-well culture plates. Confluent monolayer was scratched using a 200 μl pipette tips and medium replaced with fresh medium to remove cell debris. Cells were allowed to grow for 48 h. Photographs were taken with an inverted microscope (Olympus, Tokyo, Japan). Digital straight lines were drawn on the borders of scratches and distance of cell growth with time was recorded.

2.8. Preparation of RNA-Seq libraries

Total RNA was purified from MELFs of *Dip2b*^{+/+}, *Dip2b*^{+/-} and *Dip2b*^{-/-} using RNAiso plus reagent (Takara, Dalian, China) according to manufacturer's protocol. RNA concentration and quality were determined using NanoDrop 2000 (Thermo Fisher Scientific, USA) and Bioanalyzer (Agilent Technologies, USA). Messenger RNA was purified using oligo (dT)-attached magnetic beads, fragmented before cDNA Synthesis.

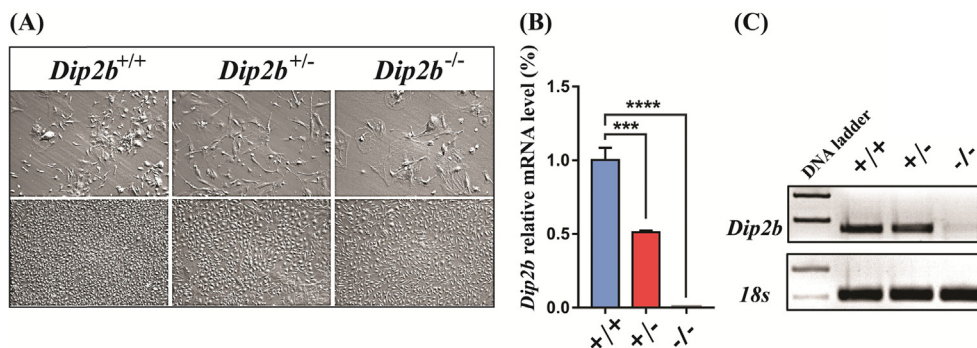


Fig. 1. MELF cell isolation and *Dip2b* mRNA expression analysis by qPCR (A) Cell images of MELF cultures at low (Top panel) and high (Bottom panel) density. (B) Relative expression levels of *Dip2b* mRNA in MELFs by qPCR. (C) Gel electrophoresis image showing PCR products.

Table 1
Summary of sequencing data processing.

| Sample | Total Mapping (%) | Uniquely Mapping (%) |
|-----------------------------|-------------------|----------------------|
| <i>Dip2b</i> ^{+/+} | 97.06 | 79.67 |
| <i>Dip2b</i> ^{+/-} | 97.08 | 80.82 |
| <i>Dip2b</i> ^{-/-} | 96.98 | 81.42 |

2.9. RNA-Seq data processing and identification of differentially expressed genes (DEGs)

Low quality reads, adaptor-only and reads with more than one unknown base (N) were removed through SOAPnuke software [11] to obtain clean reads. Q20 (%), Q30 (%) and GC content (%) were calculated. More than 1.14 Gigabyte clean reads were obtained as FASTQ format from each library. Reads were assembled into longer transcripts and mapped to reference genome using HISAT (Hierarchical Indexing for Spliced Alignment of Transcripts) [12] and Bowtie2 tool [13].

The level of transcripts was quantified and presented as paired-end RNA-Seq FPKM (Fragments Per Kilobase per Million mapped reads) normalized reads. Differentially expressed genes (DEGs) were identified by comparison of two different libraries using Position distribution [14] and Expectation-Maximization (RSEM) softwares [15].

2.10. Gene ontology and Kyoto Encyclopedia of genes and genome pathways analysis

DEGs with FDR of ≤ 0.01 and absolute value of FC ≥ 2 (Two-fold change) were considered significant for further analysis. Gene ontology (GO) annotation enrichment analysis of DEGs was implemented using Goseq R package software and estimated by hypergeometric test. DEGs were also used to identify the enriched Kyoto Encyclopedia of Genes and Genome (KEGG) pathways [16].

2.11. Validation of RNA-Seq results by quantitative real-time PCR (qPCR)

One μg of total RNA was reverse-transcribed into first-strand complementary DNA (cDNA) with Prime Script RT Reagent Kit

Table 2
Statistical summary of filtered reads.

| Sample | Total Raw Reads (M) | Total Clean Reads (M) | Total Clean Bases (Gb) | Clean Reads Q20 | Clean Reads Q30 | Clean Reads Ratio |
|-----------------------------|---------------------|-----------------------|------------------------|-----------------|-----------------|-------------------|
| <i>Dip2b</i> ^{+/+} | 23.38 | 22.7 | 1.14 | 99.12 | 96.3 | 97.1 |
| <i>Dip2b</i> ^{+/-} | 23.51 | 22.92 | 1.15 | 99.19 | 96.75 | 97.5 |
| <i>Dip2b</i> ^{-/-} | 23.44 | 22.81 | 1.14 | 99.1 | 96.55 | 97.3 |

(Perfect Real Time, TaKaRa, Dalian, China) according to the manufacturer's instructions. Quantitative real-time PCR (qPCR) was performed with 50 ng of cDNA using One-Step SYBR PrimeScript™ RT-PCR kit (Takara, Dalian, China). All reactions were performed in triplicate. All primers were initially evaluated for efficiency using relative standard curve and electrophoresis on gel.

2.12. Statistical analysis

Statistical analysis was performed using GraphPad Prism 5.01 (GraphPad Software Inc). Significant differences between groups were evaluated using Student's *t* test. *P*-values were two-sided and *P*-values < 0.05 was considered statistically significant.

3. Results and discussion

3.1. *Dip2b* mRNA expression level of *Dip2B*-deficient MELFs

Since *Dip2b*^{-/-} mice dies postnatally and lung development seems the major cause (Supplementary Fig. 1), intercrosses of *Dip2b*^{+/-} mice were used to prepare MELFs and total RNAs from all three genotypes, *Dip2b*^{-/-}, *Dip2b*^{+/-} and *Dip2b*^{+/+} at E14.5 (Fig. 1A). *Dip2b* mRNA expression in MELFs was confirmed by quantitative real-time PCR (qPCR) (Fig. 1B, C). Results show expected decrease of *Dip2b* mRNA expression. The mRNAs from MELFs were prepared for RNA-Seq.

3.2. Gene expression profiling of MELFs under *Dip2B*

To study the potential biological role of Dip2B, three libraries were generated from *Dip2b*^{-/-}, *Dip2b*^{+/-} and *Dip2b*^{+/+} MELFs and analyzed on BGISEQ-500 platform. The raw data of RNA-Seq is accessible at the Sequence Read Archive (SRA) database in NCBI with the following link (<https://www.ncbi.nlm.nih.gov/bioproject/PRJNA647133/>) under the accession number PRJNA647133. Clean reads were mapped to *Mus musculus* reference genome (GRCm38.p6/NCBI, GCF_000001635.26). As shown in Table 1, ~97% of total mapping was acquired and >80% was uniquely mapped, indicating the reliability of sequencing data. Table 2 is summarizing the sequencing reads among samples. Normalized FPKM was calculated and expression level distribution shown in (Supplementary

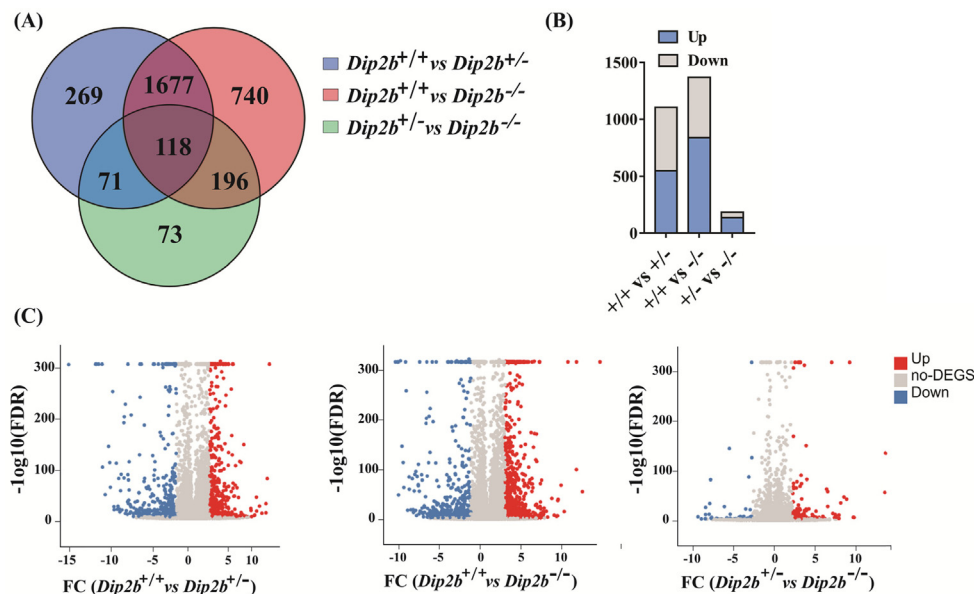


Fig. 2. Overview of gene expression profiling. (A) Venn diagram showing unique and overlapping DEGs between homozygous and heterozygous MELFs (FC ≥ 1 and FDR ≤ 0.001). (B) Number of up- and down-regulated DEGs in *Dip2b*^{-/-} and *Dip2b*^{+/-} vs *Dip2b*^{+/+} (C) Volcano plots highlighting significant DEGs among three comparative samples. Each dot in plot corresponds to one differentially expressed gene, the y-axis represents $-\log_{10}(\text{FDR})$ and the x-axis displays the differences of FC values in samples. Blue and red dots represent up- and down-regulated differentially expressed genes, whereas gray dots indicate genes with no change. (For interpretation of the references to colour in this figure legend, the reader is referred to the web version of this article.)

Fig. 2A). The overlapped genes were identified 1677 and 118 genes differentially expressed in both homozygous and heterozygous MELFs. 269 unique DEGs were expressed in *Dip2b*^{+/-}, 740 unique DEGs were expressed in *Dip2b*^{-/-} vs *Dip2b*^{+/+} and 73 unique DEGs were expressed in *Dip2b*^{+/-} vs *Dip2b*^{-/-} MELFs respectively (Fig. 2A).

Comparisons between *Dip2b*^{-/-} vs *Dip2b*^{+/+} and *Dip2b*^{+/-} vs *Dip2b*^{+/+} identified 1369 and 1104 differentially expressed genes (DEGs) based on fold change ≥ 2 and adjusted FDR ≤ 0.01 . Among them, 839 and 549 are significantly up- and 530 and 555 significantly down-regulated (Fig. 2B). Volcano plot and heatmap are used to show the significant DEGs (Fig. 2C and Supplementary Fig. 2B). Fifty of the most up- and down-regulated DEGs are listed in Table 3 and Supplementary Table 1. Among them, six genes *Ear2*, *Entpd4*, *Fpr2*, *Hist2h3c1*, *Zfp967* and *Gm14296* are the most significantly up-regulated while 6 genes *Hmga1b*, *Havcr1*, *Pax2*, *Pax8*, *Hoxa10*, *Hoxa11* and *Hoxac10* are the most significantly down-regulated.

3.3. Gene ontology (GO) analysis of *Dip2b*-regulated DEGs.

In order to identify the potential biological roles of *Dip2b* in embryonic stages, DEGs identified from comparison of *Dip2b*-deficient and WT MELFs were used for GO analysis. GO is classified into three independent categories, biological process (BP), molecular function (MF) and cellular component (CC). Each DEG could be assigned to one or more GO terms. A total of 1369 and 1104 DEGs with FC ≥ 2 and FDR < 0.01 were identified from comparisons of *Dip2b*^{-/-} vs *Dip2b*^{+/+} and *Dip2b*^{+/-} vs *Dip2b*^{+/+} MELFs. GO analysis found 28 BP, 17 MF and 12 CC significantly annotated (Fig. 3, Supplementary Fig. 3 and Supplementary Fig. 4). Annotated BP categories include 'cell adhesion', 'cell differentiation', 'regulation of signaling receptor activity', 'multicellular organism development'. MF categories include 'ion channel activity', 'ligand-gated sodium channel activity', 'voltage-gated potassium channel activity', 'extracellular matrix structural constituent', 'calcium ion binding' and 'DNA binding transcription activity'. DEGs-annotated CC cate-

gories are 'extracellular region', 'integral component of plasma membrane', 'anchored component of plasma membrane', 'basolateral plasma membrane', 'cornified envelop', 'cell surface' and 'apical plasma membrane' (Supplementary Table 2). Based on DAVID (Database for Annotation, Visualization, and Integrated Discovery [17,18]), the functional annotation clustering tool revealed that a list of cluster terms from BP, MF, and CC categories were mainly enriched with DEGs related to membrane structure and its activities (Supplementary Table 3). All the results suggest that *Dip2b* may play important roles in cell to cell interactions, membrane integrity and membrane activities which are critical for cell differentiation and function.

Dip2b-deficient MELFs resulted in upregulation of 60 (*Dip2b*^{-/-} vs *Dip2b*^{+/+}) and 52 (*Dip2b*^{+/-} vs *Dip2b*^{+/+}) DEGs that are involved in immune system and inflammatory responses respectively. In immune system process, 43 genes were enriched in innate immune response, 14 genes in defense response to virus and 11 genes in adaptive immune response (Supplementary Table 4, Supplementary Table 5). In inflammatory response category, most of the genes are chemotaxis genes including (*Fpr2*, *Fpr1*, *Ccr2*, *Cxcl15*, *Ccl9*, *Ccl6*, *Ccl11*, *Cxcl2*, *Ccl22*, *S100a8*, *Ccl12*, *Ccr5*, *Ccl7*, *Pik3cg*, *Ccl2*, *Cxcl3*), 12 genes in neutrophil chemotaxis, 7 genes in Eosinophil chemotaxis, 8 genes in monocyte chemotaxis and 8 genes in lymphocyte chemotaxis (Supplementary Table 6), indicating the importance of *Dip2b* in regulation of cell migration in immune responses.

3.4. KEGG pathway analysis on *Dip2b*-regulated DEGs

To elucidate the potential biological pathways under *Dip2b* regulation, KEGG pathway analysis was performed for *Dip2b*-regulated DEGs. KEGG classification revealed that 'signal transduction' and 'immune system' terms have the highest number of DEGs (Supplementary Fig. 5). The Q value < 0.05 was considered significantly represented and KEGG pathways were enriched based on FC ≥ 2 and FDR < 0.01 . Top 20 most enriched pathways between *Dip2b*^{-/-} vs *Dip2b*^{+/+} and *Dip2b*^{+/-} vs *Dip2b*^{+/+} are shown in Fig. 4

and Supplementary Fig. 6. Among them, 'ko04974 protein digestion and absorption', 'ko04924 renin secretion', 'ko04972 pancreatic secretion', 'ko04060 cytokines-cytokines receptor interaction' and 'ko00140 steroid hormone synthesis' metabolism pathways are the most significantly down-regulated pathways, whereas 'ko04380 Osteoclast differentiation', 'ko04621 NOD-like receptor signaling pathway' and 'ko04145 Phagosome' were the most up-regulated pathways (Supplementary Table 7a and 7b). Results demonstrate that multiple pathways are under Dip2B regulation and confirms that Dip2B is important in regulating membrane activities and be involved in regulation of metabolism.

3.5. *Hox* gene family are regulated by *Dip2B*

Homeodomain proteins encoded by *Hox* genes are responsible for regulating expression of many target genes involved in cell proliferation and differentiation [19–22]. These genes are also known to be involved in cancers and controlled by DNA methylation

[23,24]. Among differentially expressed transcription factors (TFs), homeobox (*Hox*) gene family was the most dysregulated genes in *Dip2B*-deficient MELFs (38 down- and 6 up-regulated genes in both heterozygous and homozygous MELFs). Results strongly suggest that *Dip2B* may regulate embryo development and differentiation through *Hox* gene expression. *Dip2B* contains DMAP1 binding domain and may regulate *Hox* gene transcription by DNA methylation [4]. Several TFs that belong to zinc finger (zf-C2H2), basic helix-loop-helix (bHLH) and Fox proteins are also significantly dysregulated. TFs with fold change ≥ 2 and FDR < 0.01 are listed in Table 4 and Supplementary Tables 8 and 9.

3.6. *Dip2B* regulates cell proliferation

Cell proliferation is an important process during development and tissue maintenance [25]. GO analysis shows that DEGs were significantly enriched in 'GO:0008285 ~negative regulation of cell proliferation' and 'GO:0030308 ~negative regulation of cell

Table 3
The 50 most differentially expressed genes between *Dip2b*^{+/+} vs *Dip2b*^{-/-} (Fold change ≥ 2 , FDR < 0.01).

| Up-regulated genes | FC ≥ 2 | FDR | P value | Down-regulated genes | FC < 2 | FDR | P value |
|----------------------|-------------|-------------|-------------|----------------------|--------------|-----------|-----------|
| <i>Ear1</i> | 13.11374217 | 0 | 0 | <i>Pax8</i> | -10.82813648 | 2.23E-12 | 4.84E-13 |
| <i>Ear10</i> | 11.05934446 | 5.87E-53 | 4.20E-54 | <i>Pax2</i> | -10.60316268 | 6.36E-13 | 1.34E-13 |
| <i>Ear2</i> | 10.37424254 | 0 | 0 | <i>Havcr1</i> | -10.48850965 | 1.70E-104 | 6.57E-106 |
| <i>Fpr2</i> | 10.35974956 | 7.82E-95 | 3.25E-96 | <i>Sprr2f</i> | -10.46147945 | 1.11E-46 | 8.74E-48 |
| <i>Eno1b</i> | 9.370435927 | 0 | 0 | <i>Hoxa10</i> | -10.24317398 | 1.20E-302 | 1.60E-304 |
| <i>Ndufa11b</i> | 8.939579214 | 7.79E-15 | 1.50E-15 | <i>Hoxa11</i> | -10.05799172 | 1.94E-139 | 5.62E-141 |
| <i>Entpd4</i> | 8.569855608 | 2.50E-65 | 1.47E-66 | <i>Hoxd10</i> | -9.920352855 | 2.22E-108 | 8.23E-110 |
| <i>Sell</i> | 8.22881869 | 3.05E-38 | 2.83E-39 | <i>ccdc198</i> | -9.840777924 | 6.09E-61 | 3.81E-62 |
| <i>Zfp967</i> | 8.184875343 | 6.81E-36 | 6.67E-37 | <i>Hmga1b</i> | -9.63828506 | 0 | 0 |
| <i>Hamp2</i> | 8.159871337 | 9.74E-07 | 3.02E-07 | <i>Hoxc10</i> | -9.564784619 | 1.18E-245 | 1.93E-247 |
| <i>Wfdc21</i> | 8.06608919 | 1.89E-06 | 5.98E-07 | <i>Tjff1</i> | -9.398743692 | 2.19E-17 | 3.80E-18 |
| <i>Stfa1</i> | 8.027905997 | 7.06E-06 | 2.34E-06 | <i>Hoxc8</i> | -9.221587121 | 1.08E-80 | 5.25E-82 |
| <i>Hist2h3c1</i> | 7.768184325 | 6.95E-08 | 1.97E-08 | <i>Hoxc9</i> | -9.204571144 | 1.32E-57 | 8.74E-59 |
| <i>Gm14296</i> | 7.491853096 | 5.23E-40 | 4.70E-41 | <i>Hist2h3c2</i> | -9.022367813 | 2.75E-18 | 4.60E-19 |
| <i>Hist2h2aa2</i> | 7 | 3.55E-04 | 1.41E-04 | <i>Clca1</i> | -8.854868383 | 1.19E-77 | 5.97E-79 |
| <i>Adora3</i> | 6.845490051 | 2.05E-15 | 3.83E-16 | <i>Reg1</i> | -8.764871591 | 1.38E-18 | 2.28E-19 |
| <i>Evi2</i> | 6.584962501 | 1.53E-21 | 2.27E-22 | <i>Tjff2</i> | -8.717676423 | 3.48E-13 | 7.19E-14 |
| <i>Mstn</i> | 6.584962501 | 7.79E-15 | 1.50E-15 | <i>Cyp4a12b</i> | -8.632995197 | 2.87E-54 | 2.01E-55 |
| <i>Gm39743</i> | 6.539158811 | 1.75E-10 | 4.22E-11 | <i>Spaca7</i> | -8.581200582 | 8.74E-17 | 1.55E-17 |
| <i>Ang5</i> | 6.539158811 | 6.80E-04 | 2.79E-04 | <i>Hoxd11</i> | -8.558420713 | 1.49E-85 | 6.78E-87 |
| <i>Ly6k</i> | 6.491853096 | 3.55E-04 | 1.41E-04 | <i>Gsta1</i> | -8.471675214 | 4.37E-17 | 7.67E-18 |
| <i>Bmx</i> | 6.459431619 | 3.99E-15 | 7.58E-16 | <i>Pkp1</i> | -8.438791853 | 2.82E-91 | 1.21E-92 |
| <i>Cd177</i> | 6.459431619 | 1.14E-13 | 2.31E-14 | <i>Hist1h4m</i> | -8.361943774 | 3.12E-07 | 9.29E-08 |
| <i>Lipf</i> | 6.303780748 | 3.65E-06 | 1.18E-06 | <i>Gm14434</i> | -8.290018847 | 1.33E-81 | 6.36E-83 |
| <i>Gm14548</i> | 6.28128611 | 9.11E-75 | 4.75E-76 | <i>Hoxd9</i> | -8.162391329 | 1.74E-66 | 1.01E-67 |
| <i>Gm46223</i> | 6.247927513 | 4.88E-09 | 1.28E-09 | <i>Klhl1</i> | -8.154818109 | 2.26E-64 | 1.35E-65 |
| <i>LOC100041057</i> | 6.209453366 | 3.65E-06 | 1.18E-06 | <i>Clca3b</i> | -8.142107057 | 6.44E-105 | 2.47E-106 |
| <i>Ear6</i> | 6.189824559 | 3.90E-21 | 5.85E-22 | <i>Spink8</i> | -8.06608919 | 3.34E-10 | 8.17E-11 |
| <i>DXBay18</i> | 6.169925001 | 1.22E-11 | 2.75E-12 | <i>Clec18a</i> | -8.033423002 | 7.99E-54 | 5.63E-55 |
| <i>Ms4a8a</i> | 6.161887682 | 5.48E-20 | 8.53E-21 | <i>Gm8210</i> | -7.990827547 | 0 | 0 |
| <i>Gm44805</i> | 6.14974712 | 0.008947464 | 0.00428538 | <i>Il24</i> | -7.948367232 | 1.39E-15 | 2.59E-16 |
| <i>Tex45</i> | 6.132713922 | 3.28E-33 | 3.39E-34 | <i>Prr32</i> | -7.77478706 | 8.75E-14 | 1.76E-14 |
| <i>Serp1b10</i> | 6.125843933 | 2.50E-68 | 1.40E-69 | <i>Malrd1</i> | -7.768184325 | 6.05E-85 | 2.77E-86 |
| <i>Cyp4f18</i> | 6.076815597 | 7.19E-25 | 9.49E-26 | <i>Gc</i> | -7.707359132 | 1.36E-21 | 2.00E-22 |
| <i>A530032D15Rik</i> | 6.044394119 | 3.55E-04 | 1.41E-04 | <i>Dmbt1</i> | -7.693486957 | 6.44E-75 | 3.35E-76 |
| <i>LOC677525</i> | 6.044394119 | 3.55E-04 | 1.41E-04 | <i>Apela</i> | -7.607330314 | 8.46E-11 | 2.00E-11 |
| <i>Sod3</i> | 6.042856338 | 0 | 0 | <i>Hist1h3c</i> | -7.54689446 | 7.07E-05 | 2.58E-05 |
| <i>F13a1</i> | 6.005624549 | 0 | 0 | <i>Hoxd4</i> | -7.459431619 | 8.27E-26 | 1.06E-26 |
| <i>Prss16</i> | 5.930737338 | 1.34E-07 | 3.89E-08 | <i>Pmp2</i> | -7.434628228 | 1.75E-13 | 3.56E-14 |
| <i>Awat1</i> | 5.906890596 | 5.07E-05 | 1.82E-05 | <i>Gsdm2</i> | -7.400879436 | 4.25E-23 | 5.94E-24 |
| <i>Gm36504</i> | 5.882643049 | 9.74E-07 | 3.02E-07 | <i>Pitx2</i> | -7.309855263 | 2.70E-43 | 2.26E-44 |
| <i>Rnase2b</i> | 5.832890014 | 0.008942223 | 0.00428538 | <i>Kcnj16</i> | -7.235216462 | 2.60E-183 | 5.72E-185 |
| <i>2010005H15Rik</i> | 5.817623258 | 1.43E-22 | 2.04E-23 | <i>Scin</i> | -7.192292814 | 6.79E-193 | 1.41E-194 |
| <i>Gm5796</i> | 5.754887502 | 1.36E-05 | 4.64E-06 | <i>Dcdc2a</i> | -7.144266046 | 0 | 0 |
| <i>Gm9733</i> | 5.754887502 | 0.008949561 | 0.00428538 | <i>Dclk3</i> | -7.14068778 | 5.49E-243 | 9.12E-245 |
| <i>Gpr15</i> | 5.727920455 | 3.55E-04 | 1.41E-04 | <i>Spns3</i> | -7.108524457 | 3.34E-10 | 8.17E-11 |
| <i>Fhl5</i> | 5.700439718 | 0.002477977 | 0.001093626 | <i>Dnajc19-ps</i> | -7.098032083 | 2.70E-04 | 1.06E-04 |
| <i>Klrb1b</i> | 5.700439718 | 9.74E-07 | 3.02E-07 | <i>Hoxd8</i> | -7.096275911 | 1.84E-82 | 8.73E-84 |
| <i>Mcomp1</i> | 5.698247727 | 1.99E-110 | 7.28E-112 | <i>Lhx1</i> | -7.055282436 | 5.42E-21 | 8.18E-22 |
| <i>Sftpa1</i> | 5.672425342 | 6.37E-29 | 7.41E-30 | <i>Cltn</i> | -7.044394119 | 1.32E-09 | 3.34E-10 |

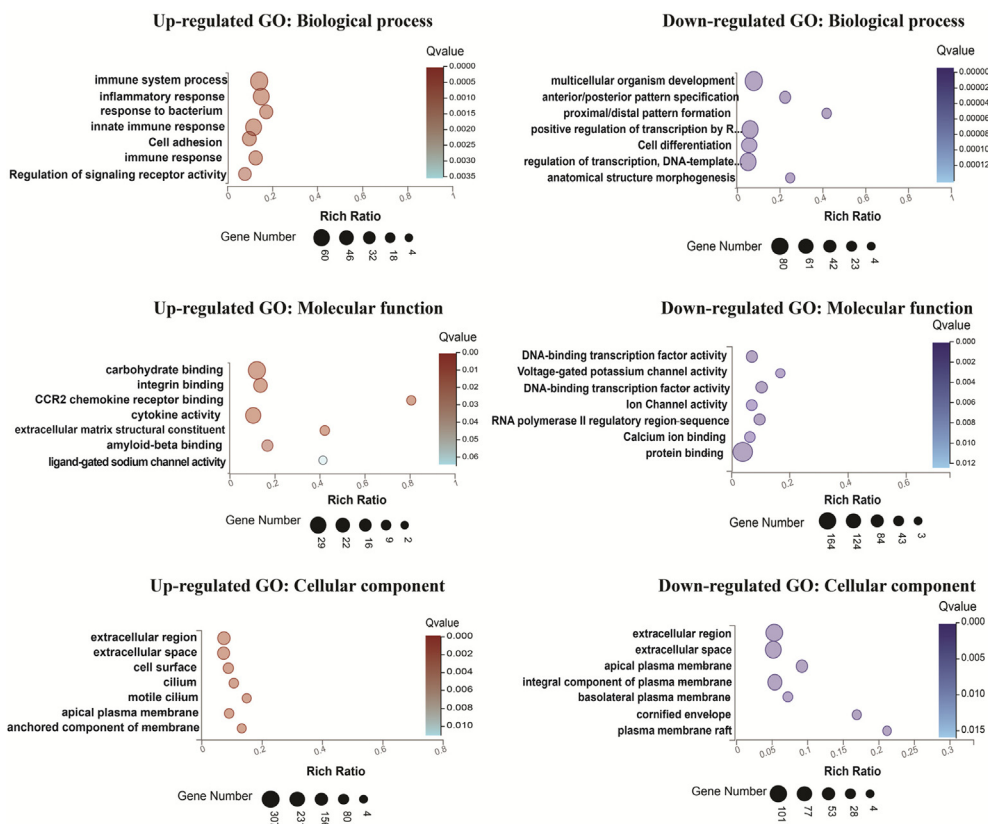
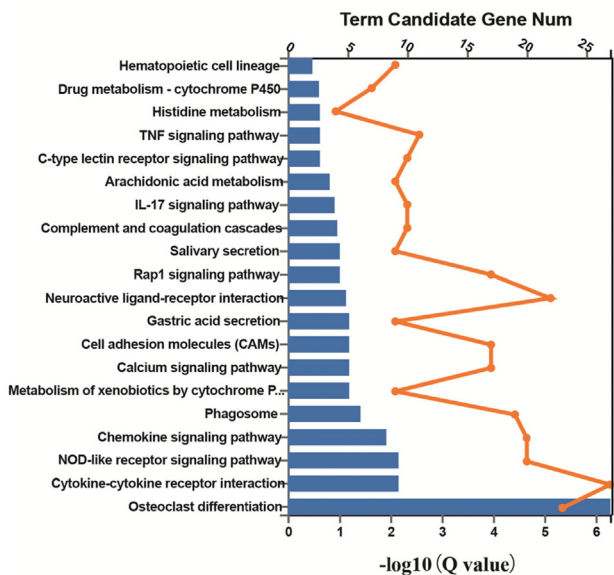


Fig. 3. GO analysis. Top seven GO terms of up- and down-regulated DEGs of *Dip2b*^{+/+} vs *Dip2b*^{-/-} (FC ≥ 2, FDR < 0.01).

Up-regulated KEGG enriched terms



Down-regulated KEGG enriched terms

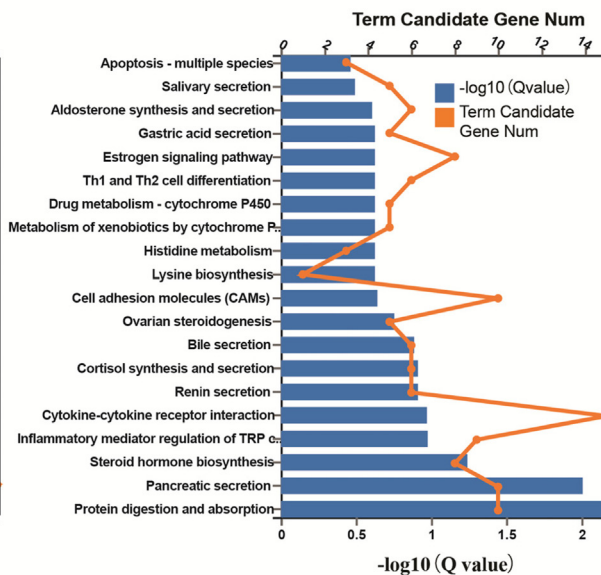


Fig. 4. KEGG pathway analysis of DEGs from *Dip2b*^{+/+} vs *Dip2b*^{-/-} MELFs. Adjusted p-values (Q-values) depicting significant enrichment (q-value < 0.05).

growth', indicating Dip2B knockout reduces cell proliferation and growth (Fig. 5A, B). Genes including *Adora3*, *Il1b*, *Sfn1* and *Nrk* [26–30] responsible for inhibition of cell proliferation were significantly up-regulated. To validate the role of Dip2B in cell proliferation, isolated MELFs were subjected to MTT viability assay. As shown in Fig. 5C, growth rates of MELFs from *Dip2b*^{-/-} and *Dip2b*^{+/-} are significantly slower than cells from *Dip2b*^{+/+} (p < 0.01), and

more obvious in *Dip2b*^{-/-} MELFs (p < 0.001). Result suggests that Dip2B may be a critical factor in regulation of cell proliferation.

3.7. *Dip2B* regulates apoptosis and cell cycle

GO analysis shows that apoptosis and cell cycle are regulated by Dip2B. Several DEGs were found significantly enriched in 'positive

Table 4
List of differentially expressed TFs between *Dip2b*^{-/-} and *Dip2b*^{+/-} (FC ≥ 2, FDR < 0.01).

| TF symbol | Number of dysregulated genes | Rich Ratio | P value | Q value |
|-----------|------------------------------|------------|----------|----------|
| Homeobox | 44 | 0.195556 | 9.21E-10 | 2.67E-08 |
| zf-C2H2 | 15 | 0.026978 | 1 | 1 |
| bHLH | 11 | 0.102804 | 0.235915 | 0.484594 |
| Fork_head | 10 | 0.227273 | 0.001856 | 0.026911 |
| HMG | 5 | 0.098039 | 0.39226 | 0.531165 |
| TF_bZIP | 4 | 0.076923 | 0.614627 | 0.742674 |
| Tub | 3 | 0.6 | 0.004512 | 0.043619 |
| ETS | 3 | 0.111111 | 0.372 | 0.531165 |
| AP-2 | 2 | 0.4 | 0.054668 | 0.396346 |
| ESR-like | 2 | 0.222222 | 0.159449 | 0.420366 |
| PAX | 2 | 0.222222 | 0.159449 | 0.420366 |
| SAND | 2 | 0.25 | 0.130642 | 0.420366 |

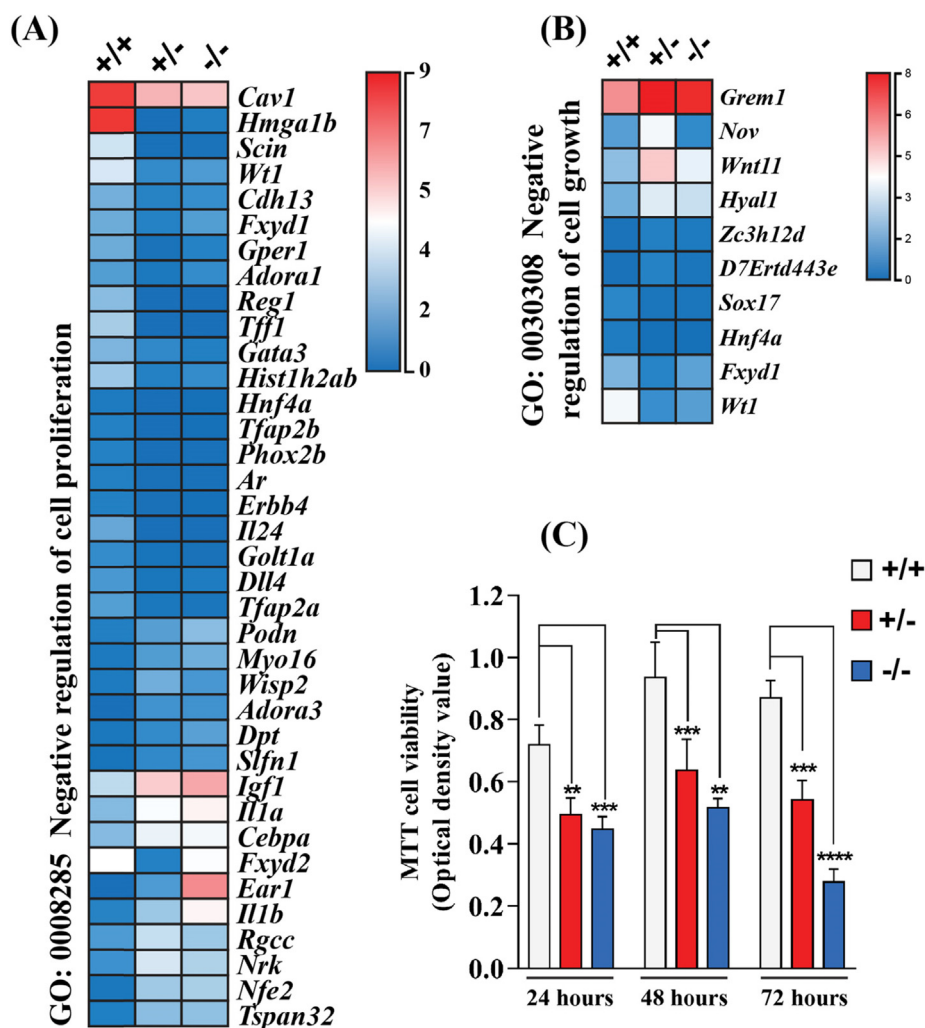


Fig. 5. Effect of Dip2B on cell proliferation and growth. Heatmap for DEGs associated with GO biological process terms of (A) 'negative regulation of cell proliferation' and (B) 'negative regulation of cell growth'. (C) MTT viability assay of MELFs derived from *Dip2b*^{-/-}, *Dip2b*^{+/-} and *Dip2b*^{+/+}.

regulation of apoptotic process', such as up-regulation of *Wnt11*, *Pycard*, *Il1b*, *Trp73*, *Clu* and *Fas* [27,31–35]. To verify whether Dip2B affects apoptosis, cells were analyzed using Annexin V and PI staining and cell cycle by flow cytometry (Fig. 6A). Results indicate that percentage of later apoptotic MELFs is significantly increased in *Dip2b*^{-/-} in comparison to *Dip2b*^{+/-} heterozygous or WT MELFs. The early apoptotic proportions in *Dip2b*^{+/-} MELFs are similar to *Dip2b*^{+/+} MELFs but increased later (Fig. 6B). *Dip2b*^{-/-} MELFs exhib-

ited an increase in G2/M population in cell-cycle profiles (Fig. 6C). Results confirm that Dip2B can significantly inhibit MELF proliferation and induce apoptosis and cell cycle arrest.

3.8. Dip2B regulates cell migration

Transcriptomic data revealed that Dip2B is involved in promotion of cell migration. Knockout of Dip2B results in significantly

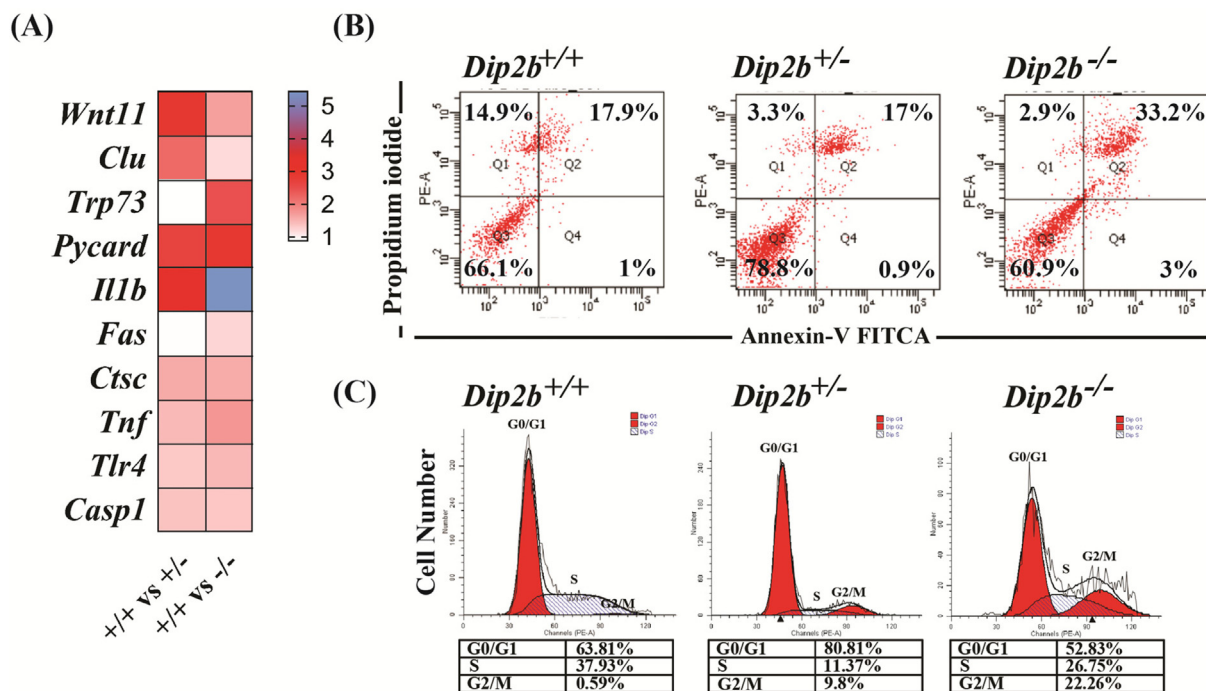


Fig. 6. Apoptosis and cell cycle analysis. (A) Heatmap for DEGs associated with GO terms 'positive regulation of apoptotic process'. (B) Apoptotic cells measured using a Becton-Dickinson FACSscan cytofluorometer. (C) Histogram of flow cytometric analysis of cell cycle showing the distribution of cell phase.

Table 5

Differentially expressed genes involved in cell migration.

| Gene symbol | <i>Dip2b</i> ^{+/+} vs <i>Dip2b</i> ^{+/-} | | | <i>Dip2b</i> ^{+/+} vs <i>Dip2b</i> ^{-/-} | | |
|----------------|--|-----------|-----------|--|-------------|------------|
| | FC ≥ 2 | FDR | P value | FC ≥ 2 | FDR | P value |
| <i>Cdh2</i> | -2.212266596 | 0 | 0 | -2.974162444 | 0 | 0 |
| <i>Podxl</i> | -1.835315003 | 5.00E-51 | 2.81E-52 | -2.297219108 | 2.88E-67 | 1.65E-68 |
| <i>L1cam</i> | -1.975442896 | 1.38E-97 | 4.16E-99 | -2.256855831 | 1.74E-115 | 6.12E-117 |
| <i>Bcar1</i> | -1.223105744 | 0 | 0 | -1.223105744 | 2.66E-05 | 3.28E-06 |
| <i>Tdgl1</i> | -6.794415866 | 2.73E-12 | 4.78E-13 | -6.794415866 | 2.73E-12 | 5.94E-13 |
| <i>Vil1</i> | -7.658211483 | 7.92E-33 | 2.30E-37 | -6.073248982 | 7.92E-33 | 8.27E-34 |
| <i>Adra2a</i> | -3.195256291 | 3.47E-108 | 3.99E-85 | -4.445799753 | 3.47E-108 | 1.29E-109 |
| <i>ErbB4</i> | -3.841302254 | 7.09E-24 | 5.32E-24 | -4.426264755 | 7.09E-24 | 9.66E-25 |
| <i>Tfap2a</i> | -3.145677455 | 6.38E-24 | 3.12E-21 | -3.660250628 | 6.38E-24 | 8.68E-25 |
| <i>Lgr6</i> | -2.220729372 | 1.16E-139 | 9.02E-90 | -3.42003818 | 1.16E-139 | 3.33E-141 |
| <i>Sema5b</i> | -1.247927513 | 5.76E-04 | 0.0794798 | -3.247927513 | 5.76E-04 | 2.35E-04 |
| <i>Hbegf</i> | -2.279689532 | 0 | 0 | -2.713977039 | 0 | 0 |
| <i>Cav1</i> | -2.302638712 | 0 | 0 | -2.604238401 | 0 | 0 |
| <i>Gper1</i> | -4.812498225 | 1.93E-18 | 1.58E-34 | -2.379538818 | 1.93E-18 | 3.20E-19 |
| <i>Sema3g</i> | -2.212993723 | 2.63E-06 | 1.97E-06 | -2.350497247 | 2.63E-06 | 8.44E-07 |
| <i>Podxl</i> | -1.835315003 | 2.88E-67 | 2.81E-52 | -2.297219108 | 2.88E-67 | 1.65E-68 |
| <i>Pdgfd</i> | -2.460097222 | 6.32E-90 | 4.99E-93 | -2.242945253 | 6.32E-90 | 2.74E-91 |
| <i>Sema6a</i> | -1.808903709 | 2.14E-71 | 3.83E-57 | -2.191760803 | 2.14E-71 | 1.16E-72 |
| <i>Col18a1</i> | -1.61403128 | 0 | 0 | -2.074086318 | 0 | 0 |
| <i>Sema7a</i> | -1.018378529 | 4.99E-47 | 1.49E-18 | -2.025796001 | 4.99E-47 | 3.92E-48 |
| <i>F2rl1</i> | -2.152928449 | 8.34E-270 | 1.25E-299 | -2.003572503 | 8.34E-270 | 1.23E-271 |
| <i>Fam107a</i> | -3 | 1.56E-04 | 4.89E-05 | -1.192645078 | 0.038533376 | 0.0208544 |
| <i>Ntrk3</i> | -2.237039197 | 5.97E-04 | 2.03E-04 | -1.137503524 | 0.025580458 | 0.01329282 |
| <i>Podn</i> | 2.162271429 | 3.41E-12 | 5.72E-13 | 3.402098444 | 3.81E-44 | 3.14E-45 |
| <i>Ptprf</i> | 0.567122422 | 2.89E-54 | 1.55E-55 | 1.018699606 | 1.21E-204 | 2.37E-206 |
| <i>Adora3</i> | 6.906890596 | 4.77E-16 | 6.58E-17 | 6.845490051 | 2.05E-15 | 3.83E-16 |

down-regulation of *Cdh2*, *Podxl*, *L1cam*, *Bcar1*, *Tdgl1* and *Hbegf* [36–41] that are known for promoting cell migration (Table 5). Genes including *Podn*, *Ptprf* and *Adora3* [26,42,43] responsible for inhibition of cell migration were up-regulated. To confirm the effect of Dip2B in cell migration, MELFs were allowed to grow to confluence and scratch wounds were made. Gap closing were recorded at different time points. Results show that *Dip2b*^{-/-} MELFs was significantly

slower in migration than that of *Dip2b*^{+/-} and *Dip2b*^{+/+} MELFs (Fig. 7).

3.9. Verification of RNA-Seq results

Ten important DEGs were validated by qPCR. Overall, qPCR results are highly consistent with the RNA-Seq results (Fig. 8). Primer sequences are listed in Supplementary Table 10.

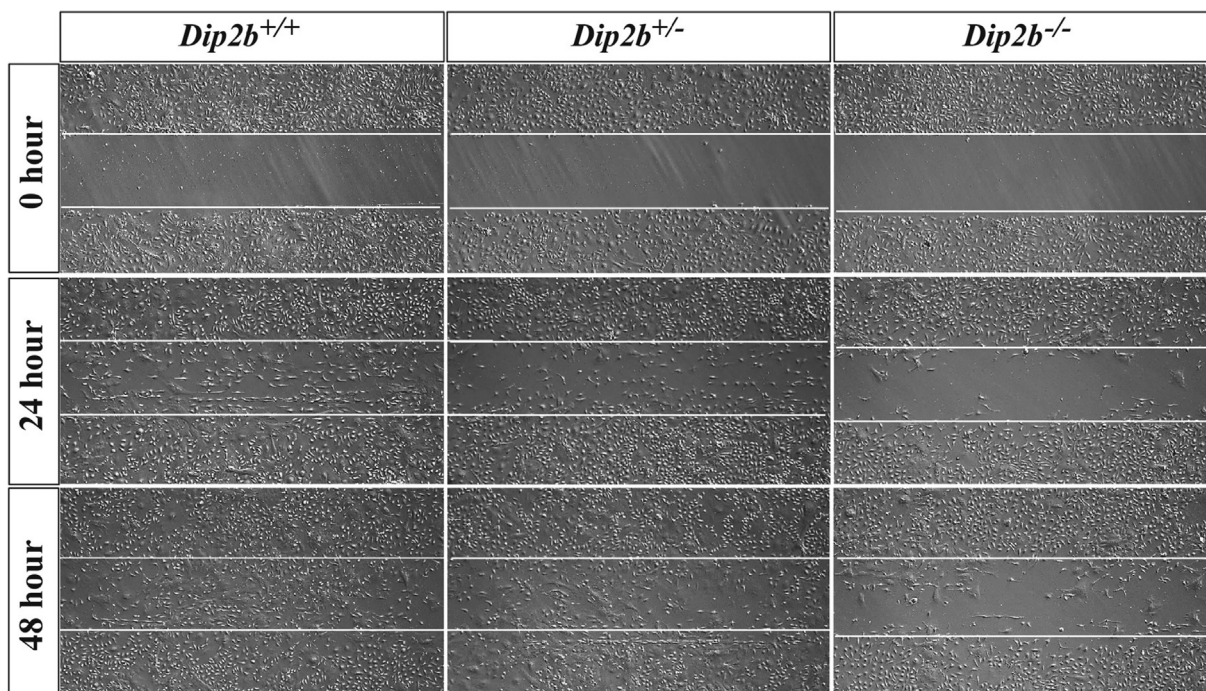


Fig. 7. Scratching assay for cell migration. Images were taken at 0, 24, 48hrs post-scratching.

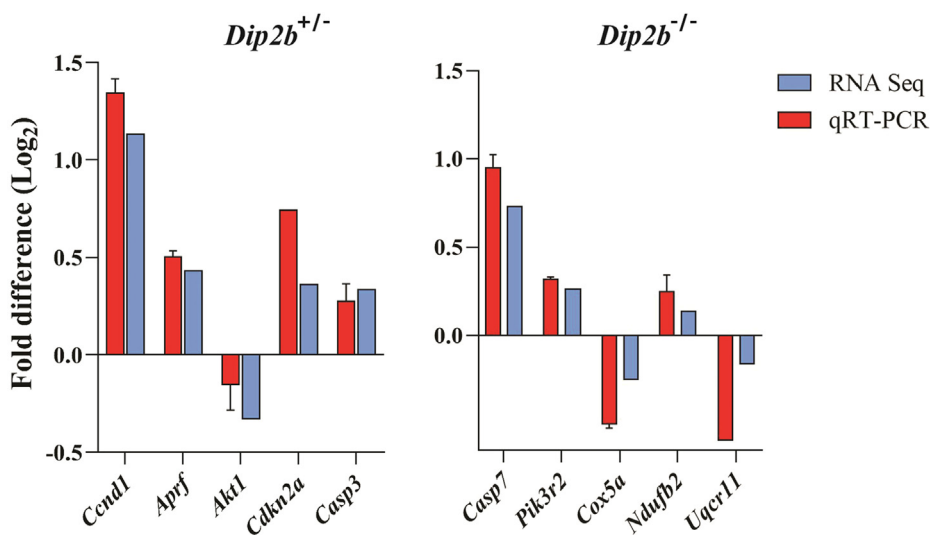


Fig. 8. Gene expression validation of DEGs from RNA-Seq by qPCR.

4. Conclusions

In this study, MELFs were isolated from *Dip2b* knockout mouse embryos at E14.5. *Dip2b*^{+/+}, *Dip2b*^{+/-} and *Dip2b*^{-/-} MELFs were examined for genome-wide gene expression. DEGs were identified and analyzed by GO and KEGG for Dip2B-regulated bioprocesses and pathways. The most enriched bioprocesses and pathways were confirmed that include cell proliferation, cell cycle, cell apoptosis and cell migration.

GO analysis showed that DEGs were mostly annotated to membrane-related GO terms including 'integral component of plasma membrane', 'anchored component of plasma membrane', 'basolateral plasma membrane', 'ion channel activity', and 'voltage-gated potassium channel activity', whereas KEGG pathways enriched

DEGs are related to metabolism including protein digestion and absorption', 'renin secretion', 'pancreatic secretion', and 'steroid hormone synthesis'. Results demonstrate that Dip2B promotes cell proliferation, increases cell migration and inhibits cell apoptosis. Knockout Dip2B leads to cell arrest at G2/M phase. Results indicate that Dip2B is involved in multiple biological processes and pathways. Dip2B may regulate many important biologic functions that are highly correlated with development, differentiation and morphogenesis. Dip2B caused upregulation of multiple genes involves in innate and adaptive immune response and inflammatory response. Our analysis has identified upregulation of potential leukocyte chemotaxis genes (*Ccl9*, *Ccl6*, *Ccl11*, *Ccl22*, *Ccl12*, *Ccr5*, *Ccl7*, *Ccl2*, *Cxcl2*, *Cxcl3*, *Cxcl15*), highlighting the potential role of Dip2B in regulation of the immune cell mobilization and inflammatory responses. A number

of transcription factors such as homeobox (*Hox*) gene family, zinc finger (zf-C2H2), basic helix-loop-helix (bHLH) and Fox proteins were found to be significantly dysregulated. The most dysregulated TFs was Homeobox (*Hox*) genes suggesting that Dip2B may regulate cell differentiation and embryo development. Together, these information are valuable for further deciphering Dip2B roles in development and disease.

Acknowledgments

We are thankful to Ms. Huiyan Wu for mouse colony management.

Funding

This work is partially supported by Natural Science Foundation of Jilin Province (20160101344JC and 20200201127JC), National Natural Science Foundation of China (81270953) and Science and Technology Project of Jilin Provincial Education Department (JJKH20180023KJ). The funders had no roles in any decision to publish or manuscript preparation.

Conflict of Interest

The authors declare that they have no competing interests.

Appendix A. Supplementary data

Supplementary data to this article can be found online at <https://doi.org/10.1016/j.csbj.2020.08.030>.

References

- Steller H, Fischbach KF, Rubin GM. disconnected: A locus required for neuronal pathway formation in the visual system of drosophila. *Cell* 1987. [https://doi.org/10.1016/0092-8674\(87\)90180-2](https://doi.org/10.1016/0092-8674(87)90180-2).
- Campos AR, Lee KJ, Steller H. Establishment of neuronal connectivity during development of the Drosophila larval visual system. *J Neurobiol* 1995. <https://doi.org/10.1002/neu.480280305>.
- Mukhopadhyay M, Pelka P, DeSousa D, Kablar B, Schindler A, Rudnicki MA, et al. Cloning, genomic organization and expression pattern of a novel Drosophila gene, the disco-interacting protein 2 (dip2), and its murine homolog. *Gene* 2002. [https://doi.org/10.1016/S0378-1119\(02\)00694-7](https://doi.org/10.1016/S0378-1119(02)00694-7).
- Winnepenninckx B, Debacker K, Ramsay J, Smeets D, Smits A, FitzPatrick DR, et al. CGG-repeat expansion in the DIP2B gene is associated with the fragile site FRA12A on chromosome 12q13.1. *Am J Hum Genet* 2007. <https://doi.org/10.1086/510800>.
- Debacker K, Frank KR. Fragile sites and human disease. *Hum Mol Genet* 2007. <https://doi.org/10.1093/hmg/ddm136>.
- Hayashi T, Lombaert IMA, Hauser BR, Patel VN, Hoffman MP. Exosomal MicroRNA transport from salivary mesenchyme regulates epithelial progenitor expansion during organogenesis. *Dev Cell* 2017. <https://doi.org/10.1016/j.devcel.2016.12.001>.
- Lv L, Zhou J, Lin C, Hu G, Yi L, Du J, et al. DNA methylation is involved in the aberrant expression of miR-133b in colorectal cancer cells. *Oncol Lett* 2015. <https://doi.org/10.3892/ol.2015.3336>.
- Ozsolak F, Milos PM. RNA sequencing: Advances, challenges and opportunities. *Nat Rev Genet* 2011. <https://doi.org/10.1038/nrg2934>.
- Pickrell JK, Marioni JC, Pai AA, Degner JF, Engelhardt BE, Nkadori E, et al. Understanding mechanisms underlying human gene expression variation with RNA sequencing. *Nature* 2010. <https://doi.org/10.1038/nature08872>.
- Singhal PK, Sassi S, Lan L, Au P, Halvorsen SC, Fukumura D, et al. Mouse embryonic fibroblasts exhibit extensive developmental and phenotypic diversity. *Proc Natl Acad Sci U S A* 2016. <https://doi.org/10.1073/pnas.1522401112>.
- Cock PJA, Fields CJ, Goto N, Heuer ML, Rice PM. The Sanger FASTQ file format for sequences with quality scores, and the Solexa/Illumina FASTQ variants. *Nucleic Acids Res* 2009. <https://doi.org/10.1093/nar/gkp1137>.
- Kim D, Langmead B, Salzberg SL. HISAT: A fast spliced aligner with low memory requirements. *Nat Methods* 2015. <https://doi.org/10.1038/nmeth.3317>.
- Langmead B, Salzberg SL. Fast gapped-read alignment with Bowtie 2. *Nat Methods* 2012. <https://doi.org/10.1038/nmeth.1923>.
- Audic S, Claverie JM. The significance of digital gene expression profiles. *Genome Res* 1997. <https://doi.org/10.1101/gr.7.10.986>.
- Li B, Dewey CN. RSEM: Accurate transcript quantification from RNA-Seq data with or without a reference genome. *BMC Bioinf* 2011. <https://doi.org/10.1186/1471-2105-12-323>.
- Kanehisa M, Araki M, Goto S, Hattori M, Hirakawa M, Itoh M, et al. KEGG for linking genomes to life and the environment. *Nucleic Acids Res* 2008. <https://doi.org/10.1093/nar/gkm882>.
- Huang DW, Sherman BT, Lempicki RA. Bioinformatics enrichment tools: Paths toward the comprehensive functional analysis of large gene lists. *Nucleic Acids Res* 2009. <https://doi.org/10.1093/nar/gkn923>.
- Huang DW, Sherman BT, Lempicki RA. Systematic and integrative analysis of large gene lists using DAVID bioinformatics resources. *Nat Protoc* 2009. <https://doi.org/10.1038/nprot.2008.211>.
- Boncinelli E. Homeobox genes and disease. *Curr Opin Genet Dev* 1997. [https://doi.org/10.1016/S0959-437X\(97\)80146-3](https://doi.org/10.1016/S0959-437X(97)80146-3).
- Cillo C, Cantile M, Faiella A, Boncinelli E. Homeobox genes in normal and malignant cells. *J Cell Physiol* 2001. <https://doi.org/10.1002/jcp.1115>.
- Holland PWH, Booth HAF, Bruford EA. Classification and nomenclature of all human homeobox genes. *BMC Biol* 2007. <https://doi.org/10.1186/1741-7007-5-47>.
- Zhao Y, Westphal H. Homeobox genes and human genetic disorders. *Curr Mol Med* 2005. <https://doi.org/10.2174/1566524023363077>.
- Li B, Huang Q, Wei GH. The role of homeobox transcription factors in cancer predisposition and progression. *Cancers (Basel)* 2019. <https://doi.org/10.3390/cancers11040528>.
- Bhatlekar S, Fields JZ, Boman BM. Role of HOX genes in stem cell differentiation and cancer. *Stem Cells Int* 2018. <https://doi.org/10.1155/2018/3569493>.
- Kaldis P. Quo Vadis cell growth and division?. *Front Cell Dev Biol* 2016. <https://doi.org/10.3389/fcell.2016.00095>.
- Ohana G, Bar-Yehuda S, Arich A, Madi L, Dreznick Z, Rath-Wolfson L, et al. Inhibition of primary colon carcinoma growth and liver metastasis by the A3 adenosine receptor agonist CF101. *Br J Cancer* 2003. <https://doi.org/10.1038/sj.bjc.6601315>.
- Maier JA, Statuto M, Ragnotti G. Endogenous interleukin 1 alpha must be transported to the nucleus to exert its activity in human endothelial cells. *Mol Cell Biol* 1994. <https://doi.org/10.1128/mcb.14.3.1845>.
- Brady G, Boggan L, Bowie A, O'Neill LAJ. Schlafen-1 causes a cell cycle arrest by inhibiting induction of cyclin D1. *J Biol Chem* 2005. <https://doi.org/10.1074/jbc.M500435200>.
- Kuang CY, Yang TH, Zhang Y, Zhang L, Wu Q. Schlafen 1 inhibits the proliferation and tube formation of endothelial progenitor cells. *PLoS ONE* 2014. <https://doi.org/10.1371/journal.pone.0109711>.
- Jin QH, He HY, Shi YF, Lu H, Zhang XJ. Overexpression of acetylcholinesterase inhibited cell proliferation and promoted apoptosis in NRK cells. *Acta Pharmacol Sin* 2004.
- Lee JM, Kim JY, Cho KW, Lee MJ, Cho SW, Kwak S, et al. Wnt11/Fgfr1b cross-talk modulates the fate of cells in palate development. *Dev Biol* 2008. <https://doi.org/10.1016/j.ydbio.2007.11.033>.
- Martino F, Hofmann K, Tschopp J. The pyrin domain: A possible member of the death domain-fold family implicated in apoptosis and inflammation. *Curr Biol* 2001. [https://doi.org/10.1016/S0960-9822\(01\)00056-2](https://doi.org/10.1016/S0960-9822(01)00056-2).
- Stiewe T, Putzer BM. Role of the p53-homologue p73 in E2F1-induced apoptosis. *Nat Genet* 2000. <https://doi.org/10.1038/82617>.
- Chaiwatanasirikul KA, Sala A. The tumour-suppressive function of CLU is explained by its localisation and interaction with HSP60. *Cell Death Dis* 2011. <https://doi.org/10.1038/cddis.2011.99>.
- Kaufmann T, Strasser A, Jost PJ. Fas death receptor signalling: roles of Bid and XIAP. *Cell Death Differ* 2012. <https://doi.org/10.1038/cdd.2011.121>.
- Bremmer F, Schallenberg S, Jarry H, Küffer S, Kaulfuss S, Burfeind P, et al. Role of N-cadherin in proliferation, migration, and invasion of germ cell tumours. *Oncotarget* 2015.
- Fernández D, Horrillo A, Alquezar C, González-Manchón C, Parrilla R, Ayuso MS. Control of cell adhesion and migration by podocalyxin. Implication of Rac1 and Cdc42. *Biochem Biophys Res Commun* 2013. <https://doi.org/10.1016/j.bbrc.2013.01.112>.
- Mechtersheimer S, Gutwein P, Agmon-Levin N, Stoeck A, Oleszewski M, Riedle S, et al. Ectodomain shedding of L1 adhesion molecule promotes cell migration by autocrine binding to integrins. *J Cell Biol* 2001. <https://doi.org/10.1083/jcb.200101099>.
- Tikhmyanova N, Little JL, Golemis EA. CAS proteins in normal and pathological cell growth control. *Cell Mol Life Sci* 2010. <https://doi.org/10.1007/s00018-009-0213-1>.
- N. Behrens A. Nkx2-5 regulates TdGF1 (Cripto) early during cardiac development. *J Clin Exp Cardiol* 2013. <https://doi.org/10.4172/2155-9880.s11-003>.
- Mine N, Iwamoto R, Mekada E. HB-EGF promotes epithelial cell migration in eyelid development. *Development* 2005. <https://doi.org/10.1242/dev.02030>.
- Devor Randolph, Giannarelli Chiara, Huang Li, Badimon Juan, Klotman Paul. Overexpression of the human form of the novel extracellular matrix protein podocan inhibits migration and proliferation of human vascular smooth muscle cells via down-regulation of the Wnt-pathway. *Am Heart Assoc* 2011:A16488.
- Soulières D, Hirsch FR, Shepherd FA, Bordogna W, Delmar P, Shames DS, et al. PTPRF expression as a potential prognostic/predictive marker for treatment with erlotinib in non-small-cell lung cancer. *J Thorac Oncol* 2015. <https://doi.org/10.1097/JTO.0000000000000624>.